ACS OMEGA

http://pubs.acs.org/journal/acsodf

Article

Boosting Phototransistor Performance in Monolayer TMDs via Multiple Reflections from DBR

Ashok Mondal, Chandan Biswas,* and Young Hee Lee*

Cite This: *ACS Omega* 2023, 8, 1677−1682

Read Online

ACCESS | Metrics & More | Article Recommendations

ABSTRACT: Transition-metal dichalcogenides (TMDs) are intensively studied for high-performance phototransistors. However, the device performance is limited by the single photoexcitation. Here, we show a unique strategy in which phototransistor performance can be boosted by fabricating the device on top of a distributed Bragg reflector (DBR). Monolayer molybdenum disulfide (MoS_2) and tungsten disulfide (WS_2) phototransistors were fabricated on DBR and SiO_2 substrates for comparison. Furthermore, phototransistor performances including photocurrent, responsivity, photoinduced mobility, and subthreshold swing highlight 582 times enhancement in photoresponsivity ratio and 350 times enhancement in photocurrent ratio in the DBR sample using transparent graphene electrode and hBN encapsulation.

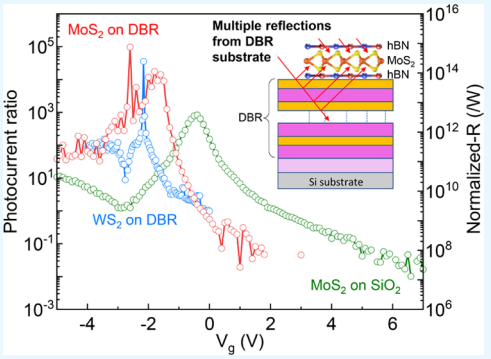

Ultrahigh exciton binding energy (up to a few hundred meV) results in a strong light−matter interaction in two-dimensional (2D) van der Waals (vdWs) layered TMDs.[1−3] In particular, one-atom-thick (∼0.7 nm) molybdenum disulfide (MoS_2) and tungsten disulfide (WS_2) exhibit direct band gap, ultrahigh photodetection, and high transistor performance and could be ideal for next-generation imaging, sensing, optical communication, optical computing, and biomedical applications.[4−7] Furthermore, two-dimensional graphene can be used as conducting optical absorbers.[8,9] One of the major bottlenecks in phototransistors is the lack of efficient management of the incident photon. A comparably insignificant research focus was employed on this aspect compared to the electrical device structure of active TMD materials.[10−14] For example, high crystallinity of TMDs, different transistor device structures, better electrical contact, and electrical Schottky contact barrier was investigated heavily to improve phototransistor performance.[4−7,10−18] In particular, the current phototransistor uses excited photons dominantly from the top of the substrate. This limits the phototransistor performance. Alternative approaches are necessary to achieve high photoexcitation and phototransistor performance.

Here, we demonstrate a novel approach for enhancing photoexcitation and phototransistor performance of the TMD active layer by fabricating the transistor on top of a DBR reflector. Single photoillumination on the device results in multiple reflections from the half DBR (h-DBR) substrate and, consequently, phototransistor performance was boosted compared to the non-DBR substrate. In this novel approach, both TMD materials (MoS_2 and WS_2) showed improved phototransistor properties on DBR substrates compared to conventional SiO_2 substrates. Furthermore, optically transparent graphene and hexagonal boron nitride (hBN) were used as a gate electrode, gate dielectric, and encapsulation layer for uninterrupted photon transport during device operation. Phototransistor properties are investigated in detail using different electrical fields and temperature conditions. Our results clearly demonstrate that the boosted phototransistor performance can be achieved using the DBR substrate approach.

DBR was fabricated using a low-refractive-index material (n = 1.46 of SiO_2) and another high-refractive-index (n = 2.16 of Ta_2O_5) material consecutively using an e-beam evaporation system.[19,20] To achieve DBR reflectance close to 100% and a DBR window covering the MoS_2 absorption energy, 12.5 pairs of consecutive SiO_2/Ta_2O_5 layers were optimized with SiO_2 thickness around 114 nm and Ta_2O_5 thickness around 81 nm, respectively. Similarly, SiO_2 thickness of 108 nm and Ta_2O_5 thickness of 73 nm were optimized for WS_2. All two-dimensional (2D) materials such as MoS_2, WS_2, hBN, and graphene were obtained by the conventional mechanical exfoliation method. The transistor was fabricated by starting with the graphene gate electrode transfer using a dry transfer method described elsewhere.[21] This aligned dry transfer

Received: November 23, 2022
Accepted: December 14, 2022
Published: December 22, 2022

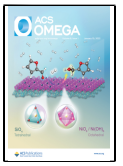

method was also utilized to transfer hBN (15 nm) and TMD (monolayer) layers on top of the graphene gate electrode. Metal electrodes (Ti/Au of 5/50 nm) were fabricated on top of the contact region using an e-beam lithograph, followed by a standard RF-sputtering deposition system. A ∼5 nm thick hBN layer was transferred on top of the device at the end for device encapsulation. The electrical measurements were carried out in a closed-cycle refrigerator with 488 nm and 5.26 mW laser excitations.

hBN-encapsulated MoS_2 on an hBN substrate (hBN-MoS_2-hBN) shows stable and improved electrical performance.[22] Therefore, the hBN-MoS_2-hBN heterostructure on a DBR substrate incorporates multiple photon reflections from the DBR to enhance phototransistor performance (schematically represented in Figure 1a). Figure 1b shows the optical micrograph of the fabricated hBN-MoS_2-hBN heterostructure on the DBR substrate. The top (blue) and bottom (green) hBN were marked with dotted lines for clarity. The monolayer MoS_2 region was selected (red circle) for optical characterizations (demonstrated later). The cross-sectional scanning electron microscopy (SEM) micrograph of the DBR substrate is represented in Figure 1c. Consecutive SiO_2 and Ta_2O_5 layers were verified by the different contrasts in the image. Figure 1d shows the reflectance spectrum of the DBR substrate. Almost 100% reflectance was verified between 1.7 and 2.0 eV optical window, confirming the inclusion of the MoS_2 absorption energy close to 1.9 eV. Figure 1e represents the photoluminescence (PL) spectra of the monolayer MoS_2 on DBR (red) and 300 nm thick SiO_2 substrate (black). Typical A-exciton (∼1.82 eV) and B-exciton (∼1.97 eV) peaks in the monolayer MoS_2 on the SiO_2 substrate were observed due to the near band edge and deep-band excitation, respectively.[23,24] On the contrary, MoS_2 on the DBR substrate exhibits a PL peak near 1.86 eV consistent with the optical window at the center of the DBR reflectance. A prominent A-exciton peak shoulder (marked by the blue arrow) suggested the presence of neutral A-exciton near 1.82 eV. It should be noted that the PL peak position and intensity were strongly influenced by the DBR reflectance window central (DBR-induced A-exciton marked in Figure 1e). The photogenerated excitons on the DBR substrate clearly fall inside the DBR optical window as shown in Figure 1d,e. A weak A-exciton peak in MoS_2 (blue arrow in Figure 1e) near 1.82 eV suggests a strong coupling (∼1.86 eV) of the photogenerated excitons on the DBR substrate.

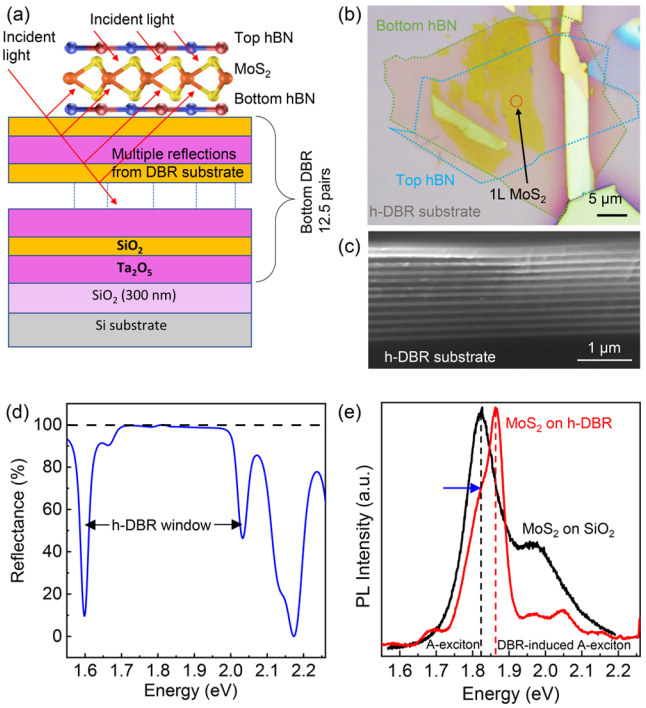

Figure 1. Device strategy for boosting TMD-based phototransistor performance using an h-DBR substrate. (a) Schematic diagram of the hBN-MoS_2-hBN monolayer heterostructure on a DBR substrate incorporating multiple photon reflections from the DBR to enhance phototransistor performance. (b) Optical micrographic image of the heterostructure on an h-DBR substrate. (c) SEM image of the DBR substrate. (d) Reflectance spectroscopy of the DBR substrate demonstrates the optical energy window. (e) PL spectra of the monolayer MoS_2 on DBR and 300 nm thick SiO_2 substrate.

The phototransistor performance of a reference control device (MoS_2 phototransistor on 300 nm thick SiO_2 substrate) is demonstrated in Figure 2a–f. Figure 2a,b shows the device structure and optical micrograph image, respectively. Gate-dependent transfer characteristics (I_d–V_g) of the device are shown in Figure 2c in dark conditions at 17 K. The device shows typical n-type characteristics of MoS_2 with an on/off ratio of around 10^6 (at V_d = 1 V). Photoexcitation on the device clearly increases I_d (solid lines in Figure 2d), showing typical phototransistor behavior of MoS_2. This was verified by changing V_d = 0.4 V. This shows similar behavior and the current change between I_d-dark and I_d-light (highlighted by the black arrow) was similar under identical photoexcitation conditions. The subthreshold swing (SS) of the device was extracted under dark and light conditions, represented in Figure 2e,f, respectively. The minimum SS (SS_{min}) was observed close to zero (V_g = −0.1 V) of around 279 mV/dec. In contrast, SS_{min} was shifted toward a higher negative V_g (−1 V), suggesting the shift of the charge neutrality due to photoexcitation. Consequently, the SS_{min} value was increased to 540 mV/dec, as shown in Figure 2f. The phototransistor performance of an identical MoS_2 device on the DBR substrate was much higher as demonstrated in Figure 2g–l. Figure 2g,h shows the device structure and optical micrograph of the MoS_2 device on the DBR substrate, respectively. The corresponding I_d–V_g graph is represented in Figure 2i, showing a lower off-current level (10^{-15} A) compared to the SiO_2 device. Interestingly, a much higher photocurrent on/off ratio was observed (highlighted by the black arrow in Figure 2j) compared to the SiO_2 device (Figure 2d). This enhancement in the photocurrent on/off ratio strongly suggests the phototransistor performance enhancement due to multiple reflections of the incoming light from the DBR substrate. The SS_{min} values were similar to the SiO_2 device for both dark (113 mV/dec) and light (519 mV/dec) conditions (see Figure 2k,l).

The photocurrent ($I_{Ph} = I_{light} - I_{dark}$) and responsivity ($R = I_{Ph}/PA$, where P = light power over area A) enable us to determine the I_{Ph} ratio ($(I_{light} - I_{dark})/I_{dark}$) and normalized-R ($I_{Ph}$ ratio/PA), respectively. The device dimensions (channel length ≈ 14 μm) and device structures for all SiO_2 and DBR devices were kept identical for direct comparison. This enabled us to compare all device performances from different devices to conclusively extract DBR substrate effects compared to SiO_2 reference devices. Figure 3a compares the I_{Ph} ratio and R ratio of both DBR and SiO_2-based samples at 17 K. DBR sample shows around 203 times higher I_{Ph} ratio and 338 times higher

https://doi.org/10.1021/acsomega.2c07518
ACS Omega 2023, 8, 1677−1682

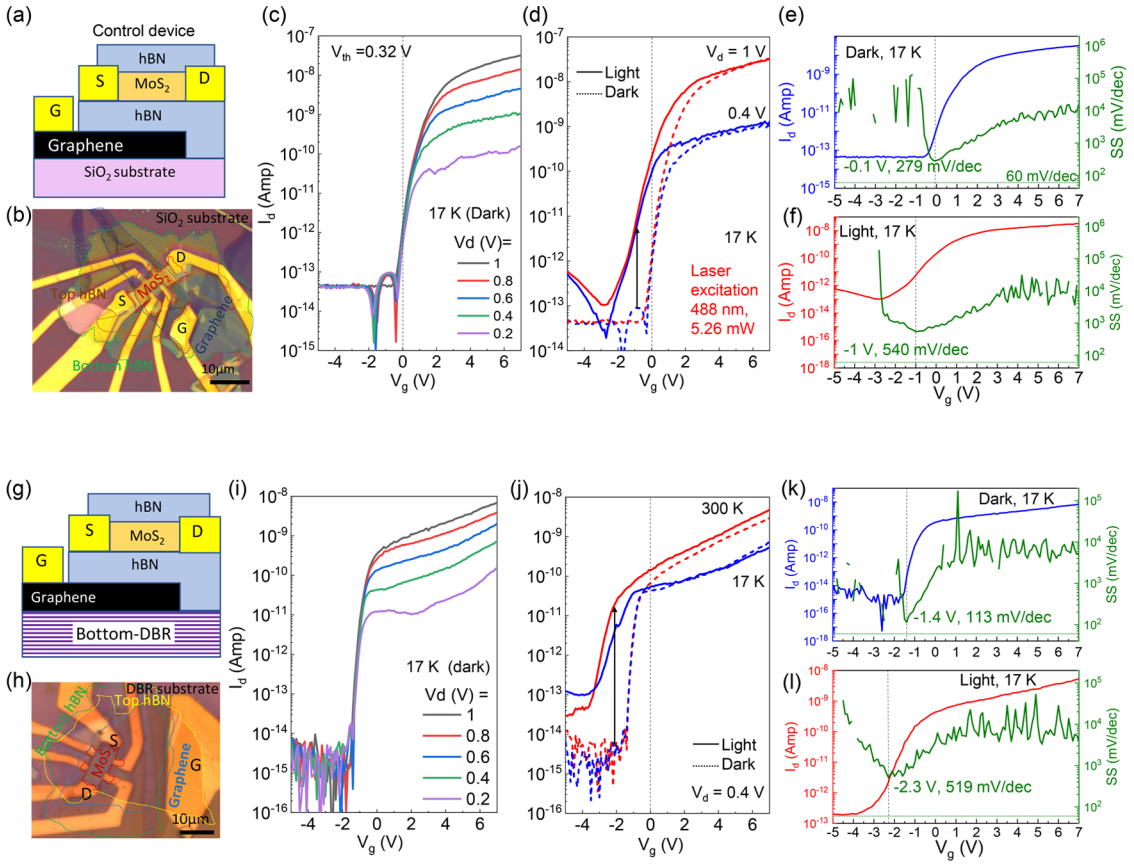

Figure 2. Phototransistor performance of a monolayer MoS_2 on 300 nm thick SiO_2 and DBR substrate: (a) schematic diagram of the device structure. (b) OM image of the fabricated device. (c) Transfer characteristics (I_d−V_g) of the device under dark conditions. (d) Phototransistor performance of the device under different source−drain voltages. (e, f) Subthreshold swing (SS) variations of the device under dark and light conditions, respectively. (g, h) Schematic diagram and OM image of the device, respectively. (i) Transfer characteristics of the device under dark conditions. (j) Phototransistor performance of the device under different temperatures. (k, l) SS variations of the device under dark and light conditions, respectively.

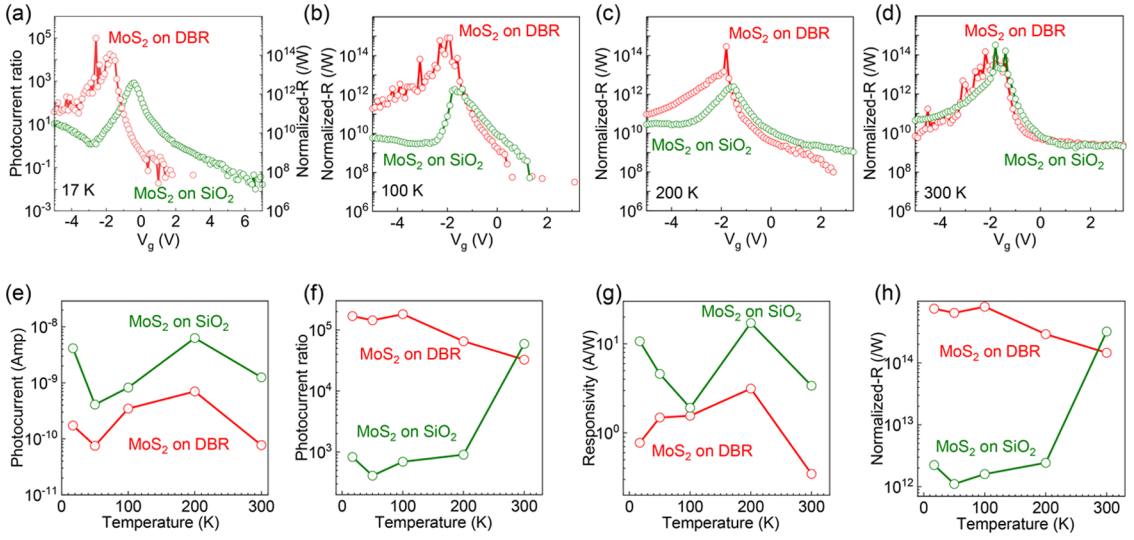

Figure 3. Comparison of all phototransistor performance parameters at different temperatures. (a) Photocurrent and responsivity ratio comparison at 17 K. (b−d) Responsivity ratio variations at 100, 200, and 300 K, respectively. (e) Photocurrent, (f) photocurrent ratio, (g) responsivity, and (h) responsivity ratio variations under different temperatures for both samples.

normalized-R compared to the SiO_2 sample. This was achieved by the incorporation of multiple photoexcitation of the MoS_2 phototransistor from the DBR substrate. The normalized-R was elevated at 100 K (508 times higher R ratio) in the DBR sample (Figure 3b). The highest I_{Ph} ratio and normalized-R of 350 and 582 W^{-1}, respectively, were observed at 50 K. However, with the increasing temperature, the normalized-R decreases (120 times at 200 K, Figure 3c) and almost becomes

https://doi.org/10.1021/acsomega.2c07518
ACS Omega 2023, 8, 1677−1682

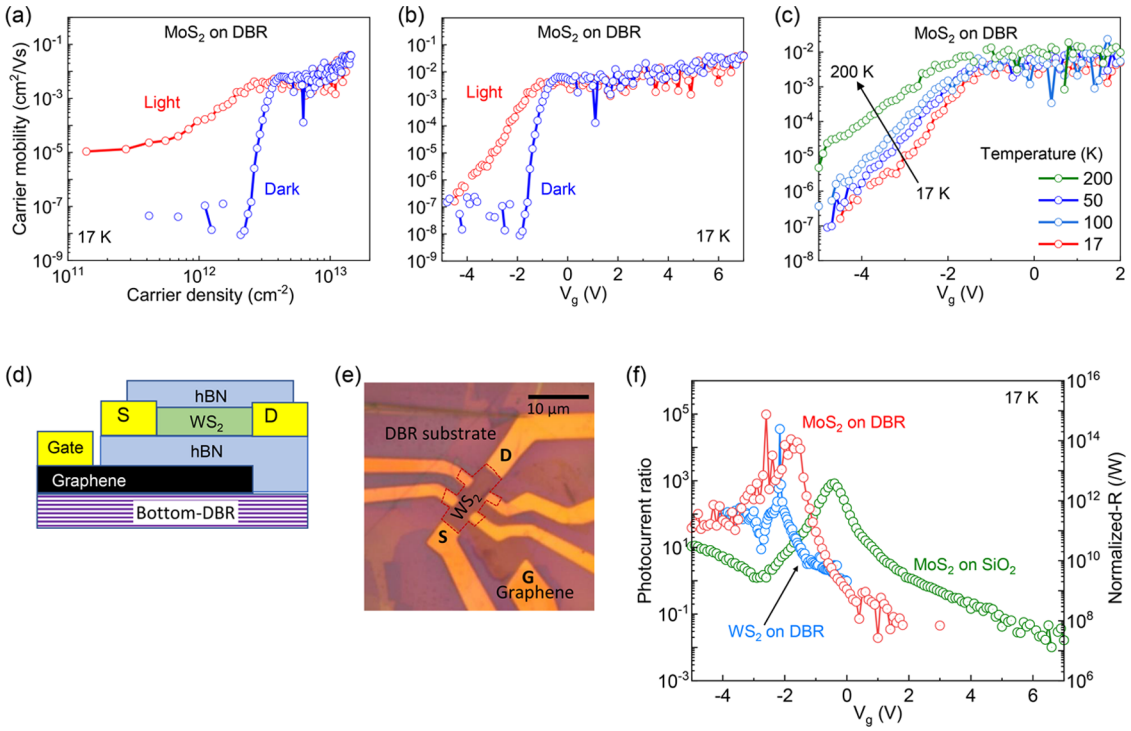

Figure 4. Phototransistor performance of a monolayer MoS_2 and WS_2 transistors on the DBR substrate w.r.t. MoS_2 on SiO_2 substrate. (a) Mobility vs carrier density comparison at 17 K under dark and light conditions. (b) The corresponding mobility variations with V_g. (c) Photoinduced carrier mobility (in light conditions) variations with V_g at different temperatures. (d, e) Schematic diagram and OM image of the device, respectively. (f) Photocurrent and responsivity ratio comparison of all samples in different V_g.

identical to the SiO_2 sample at room temperature (0.45 times at 300 K, Figure 3d). All phototransistor performance parameters (such as I_{Ph}, I_{Ph} ratio, R, and normalized-R) were compared at different temperatures for both samples (Figure 3e−h). It Is evident from Figure 3e that, the photocurrent stays nearly flat throughout the whole temperature range for both samples. However, I_{Ph} ratio decreased sharply in the SiO_2 sample at 200 K and remained flat at lower temperatures (Figure 3f). In contrast, I_{Ph} ratio increases gradually up to 100 K in the DBR sample and remains almost flat at lower temperatures. This phenomenon is drastically different from traditional non-DBR-based phototransistors.[4−7] The reduction in electron−phonon scattering with the reduction in temperatures could be the reason behind these observations and further investigations are required. A similar tendency was observed for R dependence with temperature (Figure 3g,h). R stays nearly flat throughout the whole temperature range for both samples. Furthermore, normalized-R increased in the DBR sample and decreased in the SiO_2 sample with reduced temperatures. These observations clearly highlight that the phototransistor performance (I_{Ph} ratio and normalized-R) was improved under low-temperature conditions (Figure 3f,h) in MoS_2 on the DBR substrate compared to the SiO_2-based device.

The carrier mobility vs carrier density plot (Figure 4a) clearly shows almost identical mobility near the on state (density ∼ 10^{13} cm^{-2}) in the DBR sample. However, the mobility sharply decreases in the off state of the device under dark conditions. In contrast, photogenerated carriers still persist under illumination, resulting in higher mobilities under the light condition in the off state. The V_g-dependent mobility plot clarifies the picture (Figure 4b). Figure 4c compares the V_g-dependent mobility at different temperatures under light conditions. Mobility values (in the off state) increase with increasing temperatures, and almost remain identical in the on state of the device. These observations clearly suggest that the enhancement of the photogenerated carrier mobility dominates at higher temperatures under gate-modulated low-carrier-density region (negative V_g). To verify our observations with other TMDs, a WS_2 phototransistor was fabricated on the DBR substrate with an identical device structure to the previous MoS_2 phototransistor. Figure 4d,e shows the device structure and optical micrograph of the WS_2-based devices, respectively. Figure 4f summarizes the I_{Ph} ratio and normalized-R compared to MoS_2 phototransistors on DBR and SiO_2 substrates. It is evident from the plot that the DBR devices showed higher I_{Ph} ratio and normalized-R for both TMDs (MoS_2, WS_2) phototransistors compared to the SiO_2-based device. WS_2 device exhibits a I_{Ph} ratio of around 35,612 (normalized-R ∼ 1.6×10^{14}), 43 times higher I_{Ph} ratio (72 times higher normalized-R) compared to that of the SiO_2-based device. On the other hand, the MoS_2 device exhibits 203 times higher I_{Ph} ratio (338 times higher normalized-R) compared to that of the SiO_2-based device. These results suggest an enhancement in the TMD phototransistor performance (both MoS_2 and WS_2) due to the incorporation of multiple photoexcitation from the DBR substrate compared to the SiO_2-based device. The above observations suggest that the I_{Ph} ratio and normalized-R in a conventional SiO_2-based phototransistor device architecture were dominant by the photoexcitation from the top of the TMD materials. The photoexcitation from the bottom side of the TMD was drastically limited by the poor photon reflection efficiency of the SiO_2 substrate compared to a highly reflective DBR substrate. In contrast, nearly 100% (Figure 1d) of photons were reflected by the DBR substrate, resulting in extremely

https://doi.org/10.1021/acsomega.2c07518
ACS Omega 2023, 8, 1677−1682

high photoexcitation both from the top and bottom sides of the TMD materials (see Figure 1a). Consequently, the performance (photocurrent ratio and normalized responsivity) of the TMD-based phototransistors on a DBR substrate were significantly higher than that of the conventional SiO_2-based substrate.

Phototransistor performance was boosted in TMD-based devices utilizing multiple reflections from the DBR substrate. Nearly 582 times enhancement in photoresponsivity ratio and 350 times enhancement in photocurrent ratio were observed in the DBR sample compared to SiO_2-based devices. The temperature-dependent investigation highlights improved phototransistor performance and low temperature compared to the traditional SiO_2-based devices. Furthermore, an identical WS_2 device shows similar observations, confirming the phototransistor performance enhancement for both TMDs (MoS_2 and WS_2). These results clearly demonstrate that the existing phototransistor performance can be further enhanced using our approach.

AUTHOR INFORMATION

Corresponding Authors

Chandan Biswas − *Center for Integrated Nanostructure Physics, Institute for Basic Science, Sungkyunkwan University, Suwon 16419, Republic of Korea;* orcid.org/0000-0002-2083-4219; Email: chandan@skku.edu

Young Hee Lee − *Center for Integrated Nanostructure Physics, Institute for Basic Science, Sungkyunkwan University, Suwon 16419, Republic of Korea; Department of Energy Science and Department of Physics, Sungkyunkwan University, Suwon 16419, Republic of Korea;* orcid.org/0000-0001-7403-8157; Email: leeyoung@skku.edu

Author

Ashok Mondal − *Center for Integrated Nanostructure Physics, Institute for Basic Science, Sungkyunkwan University, Suwon 16419, Republic of Korea; Department of Energy Science, Sungkyunkwan University, Suwon 16419, Republic of Korea;* orcid.org/0000-0002-4188-7184

Complete contact information is available at: https://pubs.acs.org/10.1021/acsomega.2c07518

Author Contributions

A.M. and C.B. developed the idea. C.B. and Y.H.L. supervised the project. A.M., C.B., and Y.H.L. designed the experiments. A.M. carried out the device fabrication and performed the electrical characterization supervised by C.B. A.M., C.B., and Y.H.L. wrote the manuscript.

Notes

The authors declare no competing financial interest.

ACKNOWLEDGMENTS

This work was supported by the Institute for Basic Science of Korea (IBS-R011-D1).

REFERENCES

(1) Ramasubramaniam, A. Large Excitonic Effects in Monolayers of Molybdenum and Tungsten Dichalcogenides. *Phys. Rev. B* **2012**, *86*, No. 115409.

(2) Hanbicki, A. T.; Currie, M.; Kioseoglou, G.; Friedman, A. L.; Jonker, B. T. Measurement of High Exciton Binding Energy in the Monolayer Transition-Metal Dichalcogenides Ws_2 and Wse_2. *Solid State Commun.* **2015**, *203*, 16−20.

(3) Sebait, R.; Biswas, C.; Song, B.; Seo, C.; Lee, Y. H. Identifying Defect-Induced Trion in Monolayer Ws_2 Via Carrier Screening Engineering. *ACS Nano* **2021**, *15*, 2849−2857.

(4) Wadhwa, R.; Agrawal, A. V.; Kumar, M. A Strategic Review of Recent Progress, Prospects and Challenges of Mos_2-Based Photodetectors. *J. Phys. D: Appl. Phys.* **2021**, *55*, No. 063002.

(5) Taffelli, A.; Dirè, S.; Quaranta, A.; Pancheri, L. Mos_2 Based Photodetectors: A Review. *Sensors* **2021**, *21*, No. 2758.

(6) Nalwa, H. S. A Review of Molybdenum Disulfide (Mos_2) Based Photodetectors: From Ultra-Broadband, Self-Powered to Flexible Devices. *RSC Adv.* **2020**, *10*, 30529−30602.

(7) Mu, C.; Xiang, J.; Liu, Z. Photodetectors Based on Sensitized Two-Dimensional Transition Metal Dichalcogenides—a Review. *J. Mater. Res.* **2017**, *32*, 4115−4131.

(8) Shangguan, Q.; Chen, Z.; Yang, H.; Cheng, S.; Yang, W.; Yi, Z.; Wu, X.; Wang, S.; Yi, Y.; Wu, P. Design of Ultra-Narrow Band Graphene Refractive Index Sensor. *Sensors* **2022**, *22*, No. 6483.

(9) Chen, H.; Chen, Z.; Yang, H.; Wen, L.; Yi, Z.; Zhou, Z.; Dai, B.; Zhang, J.; Wu, X.; Wu, P. Multi-Mode Surface Plasmon Resonance Absorber Based on Dart-Type Single-Layer Graphene. *RSC Adv.* **2022**, *12*, 7821−7829.

(10) Li, X.; Tao, L.; Chen, Z.; Fang, H.; Li, X.; Wang, X.; Xu, J.-B.; Zhu, H. Graphene and Related Two-Dimensional Materials: Structure-Property Relationships for Electronics and Optoelectronics. *Appl. Phys. Rev.* **2017**, *4*, No. 021306.

(11) Marin, J. F. G.; Unuchek, D.; Watanabe, K.; Taniguchi, T.; Kis, A. Mos_2 Photodetectors Integrated with Photonic Circuits. *npj 2D Mater. Appl.* **2019**, *3*, No. 14.

(12) Kufer, D.; Nikitskiy, I.; Lasanta, T.; Navickaite, G.; Koppens, F. H. L.; Konstantatos, G. Hybrid 2d−0d Mos_2−Pbs Quantum Dot Photodetectors. *Adv. Mater.* **2015**, *27*, 176−180.

(13) Huo, N.; Gupta, S.; Konstantatos, G. Mos_2−Hgte Quantum Dot Hybrid Photodetectors Beyond 2 μm. *Adv. Mater.* **2017**, *29*, No. 1606576.

(14) Chen, Y.; Wang, X.; Wu, G.; Wang, Z.; Fang, H.; Lin, T.; Sun, S.; Shen, H.; Hu, W.; Wang, J.; Sun, J.; Meng, X.; Chu, J. High-Performance Photovoltaic Detector Based on $Mote_2$/Mos_2 Van Der Waals Heterostructure. *Small* **2018**, *14*, No. 1703293.

(15) Xie, Y.; Liang, F.; Chi, S.; Wang, D.; Zhong, K.; Yu, H.; Zhang, H.; Chen, Y.; Wang, J. Defect Engineering of Mos_2 for Room-Temperature Terahertz Photodetection. *ACS Appl. Mater. Interfaces* **2020**, *12*, 7351−7357.

(16) Lee, H. S.; Baik, S. S.; Lee, K.; Min, S.-W.; Jeon, P. J.; Kim, J. S.; Choi, K.; Choi, H. J.; Kim, J. H.; Im, S. Metal Semiconductor Field-Effect Transistor with Mos_2/Conducting Nio_x Van Der Waals Schottky Interface for Intrinsic High Mobility and Photoswitching Speed. *ACS Nano* **2015**, *9*, 8312−8320.

(17) Kallatt, S.; Nair, S.; Majumdar, K. Asymmetrically Encapsulated Vertical Ito/Mos_2/Cu_2o Photodetector with Ultrahigh Sensitivity. *Small* **2018**, *14*, No. 1702066.

(18) Long, M.; Liu, E.; Wang, P.; Gao, A.; Xia, H.; Luo, W.; Wang, B.; Zeng, J.; Fu, Y.; Xu, K.; Zhou, W.; Lv, Y.; Yao, S.; Lu, M.; Chen, Y.; Ni, Z.; You, Y.; Zhang, X.; Qin, S.; Shi, Y.; Hu, W.; Xing, D.; Miao, F. Broadband Photovoltaic Detectors Based on an Atomically Thin Heterostructure. *Nano Lett.* **2016**, *16*, 2254−2259.

(19) Dong, W. J.; Lo, N.-T.; Jung, G. H.; Ham, J.; Lee, J.-L. Efficiency Enhancement and Angle-Dependent Color Change in See-through Organic Photovoltaics Using Distributed Bragg Reflectors. *Appl. Phys. Lett.* **2016**, *108*, No. 103902.

(20) Erotokritou, K.; Heath, R. M.; Taylor, G. G.; Tian, C.; Banerjee, A.; Casaburi, A.; Natarajan, C. M.; Miki, S.; Terai, H.; Hadfield, R. H. Nano-Optical Photoresponse Mapping of Superconducting Nanowires with Enhanced near Infrared Absorption. *Supercond. Sci. Technol.* **2018**, *31*, No. 125012.

(21) Frisenda, R.; Navarro-Moratalla, E.; Gant, P.; Lara, D. P. D.; Jarillo-Herrero, P.; Gorbachev, R. V.; Castellanos-Gomez, A. Recent Progress in the Assembly of Nanodevices and Van Der Waals Heterostructures by Deterministic Placement of 2d Materials. *Chem. Soc. Rev.* **2018**, *47*, 53−68.

(22) Lee, G.-H.; Cui, X.; Kim, Y. D.; Arefe, G.; Zhang, X.; Lee, C.-H.; Ye, F.; Watanabe, K.; Taniguchi, T.; Kim, P.; Hone, J. Highly Stable, Dual-Gated Mos_2 Transistors Encapsulated by Hexagonal Boron Nitride with Gate-Controllable Contact, Resistance, and Threshold Voltage. *ACS Nano* **2015**, *9*, 7019−7026.
(23) McCreary, K. M.; Hanbicki, A. T.; Sivaram, S. V.; Jonker, B. T. A- and B-Exciton Photoluminescence Intensity Ratio as a Measure of Sample Quality for Transition Metal Dichalcogenide Monolayers. *APL Mater.* **2018**, *6*, No. 111106.
(24) Kaupmees, R.; Komsa, H.-P.; Krustok, J. Photoluminescence Study of B-Trions in Mos_2 Monolayers with High Density of Defects. *Phys. Status Solidi B* **2019**, *256*, No. 1800384.

https://doi.org/10.1021/acsomega.2c07518
ACS Omega 2023, 8, 1677−1682